

## LETTER

# Super-Resolution Imaging Method for Millimeter Wave Synthetic Aperture Interferometric Radiometer

Jianfei CHEN<sup>†,††a)</sup>, Xiaowei ZHU<sup>†</sup>, *Nonmembers*, and Yuehua LI<sup>††b)</sup>, *Member*

**SUMMARY** Synthetic aperture interferometric radiometer (SAIR) is a powerful sensors for high-resolution imaging. However, because of the observation errors and small number of visibility sampling points, the accuracy of reconstructed images is usually low. To overcome this deficiency, a novel super-resolution imaging (SrI) method based on super-resolution reconstruction idea is proposed in this paper. In SrI method, sparse visibility functions are first measured at different observation locations. Then the sparse visibility functions are utilized to simultaneously construct the fusion visibility function and the fusion imaging model. Finally, the high-resolution image is reconstructed by solving the sparse optimization of fusion imaging model. The simulation results demonstrate that the proposed SrI method has higher reconstruction accuracy and can improve the imaging quality of SAIR effectively.

**key words:** millimeter wave, synthetic aperture, imaging method, super-resolution, reconstruction

## 1. Introduction

Millimeter wave (MMW) imaging radiometers with high-resolution and penetration have been used in various applications. Among the MMW imaging systems, synthetic aperture interferometric radiometer (SAIR) is one of the popular systems [1]–[3]. Unlike the traditional real-aperture systems, SAIR utilizes some small antennas to constitute a large aperture antenna to realize high-resolution (HR) imaging observation. However, limited by the antenna array size, the number of visibility sampling points is usually small. Moreover, some observation errors are existed in the measured visibility function. And these may reduce the imaging accuracy of SAIR. Thus, various imaging algorithms have been proposed, such as FFT, Nonuniform FFT (NUFFT) [4], Gridding [5] and regularization methods [6], [7]. FFT-based methods utilize Fourier transforms to reconstruct MMW images directly. Although the reconstruction is efficient, its accuracy is poor, and is only suitable for the regular antenna arrays (such as “T” and “U” array). To overcome this deficiency, the NUFFT and Gridding methods are proposed for arbitrary array. But due to the problem of insertion and re-sampling, some unnecessary errors is inevitably introduced

to the reconstructed images. Regularization methods reconstruct the MMW images through the numerical inversion of synthetic aperture imaging model. The visibility function is used to reconstruct the images directly, which achieves better reconstruction accuracy and efficiency.

However, many SAIRs are the sparse SAIR with fewer antennas and visibility sampling points, the traditional regularization method will not be able to reconstruct the MMW image with high accuracy. To further improve the imaging accuracy of sparse SAIR, a novel super-resolution imaging (SrI) method based on super-resolution reconstruction idea is proposed in this paper. The main idea of super-resolution reconstruction is to reconstruct the HR images by fusing multiple low-resolution (LR) images. With the help of similarity, displacement and scaling between LR images, image super-resolution reconstruction can improve the accuracy of reconstructed images effectively, and has been widely used in various applications [8], [9]. Using the super-resolution reconstruction idea, we first utilize SAIR to detect the target at different observation locations for obtaining the multiple sparse visibility functions. Then the sparse visibility functions are used to construct a fusion visibility function, and the super-resolution imaging model is constructed simultaneously according to synthetic aperture imaging principle. Finally, HR MMW images are reconstructed by performing a sparse optimization to the super-resolution imaging model. The novelty of our SrI method is that the super-resolution imaging model with more known conditions (visibility samples) is established to model the imaging process of SAIR, which can effectively improve the image inversion accuracy. The simulation results demonstrate that the SrI method can reconstruct the MMW images with higher accuracy and clarity than the traditional regularization imaging method and image fusion method. The main contributions of this paper is to provide an effective method (SrI method) to improve the imaging accuracy of SAIR without changing its system structure.

## 2. Super-Resolution Imaging Method for SAIR

### 2.1 Synthetic Aperture Imaging Principle

Before discussing the SrI method, we first review the synthetic aperture imaging principle briefly. As Fig. 1 shows, the radiation source  $S$  is located on  $oxy$ , antennas  $(c, l)$  are located on  $OXY$ . The radiation source  $S$  is dispersed into  $N$  small parts, and the distance between source  $S_i$  and antennas

Manuscript received June 22, 2019.

Manuscript revised October 29, 2019.

Manuscript publicized June 12, 2020.

<sup>†</sup>The authors are with Dept. of Information Science and Engineering, Southeast University, Nanjing, China.

<sup>††</sup>The authors are with Dept. of Electronic Engineering and Optoelectronic Technology, Nanjing Univ. of Science and Technology, Nanjing, China.

a) E-mail: chenjf@njupt.edu.cn

b) E-mail: nlglyh2013@sina.cn

DOI: 10.1587/transinf.2019EDL8125

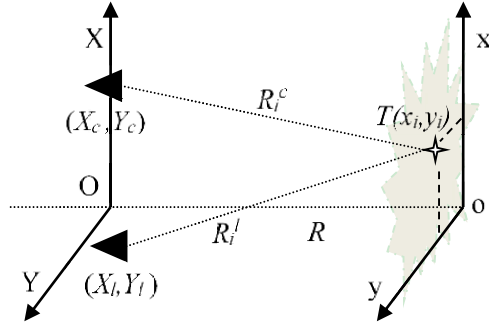


Fig. 1 Synthetic aperture imaging schematic.

is defined as  $R_i^c$  and  $R_i^l$ . The visibility samples of antenna pairs  $(c, l)$  can be represented as

$$V_{c,l} = \langle E_c(R_i^c, t) \cdot E_l^*(R_i^l, t) \rangle$$

$$= \sum_{i=0}^N T(x_i, y_i) F_c(x_i, y_i) F_l^*(x_i, y_i) r_{c,l} e^{-jk(R_i^c - R_i^l)} \quad (1)$$

where  $E_{\#}(\bullet)$  is the received signal of antenna #,  $\langle \bullet \rangle$  denotes time integration operation,  $(x_i, y_i)$  is the coordinate of radiation source  $S_i$ ,  $T(x_i, y_i)$  is the normalized brightness temperature,  $F_{\#}(\bullet)$  is the normalized antenna pattern of antenna #,  $k = 2\pi/\lambda$  is circular wave number,  $r_{c,l}$  is the fringe-wash function. Generally, the decorrelation effects are negligible and  $r_{c,l} = 1$ .  $\exp[-jk(R_i^c - R_i^l)]$  denotes the phase difference between antennas  $(c, l)$ . According to Fig. 1,  $R_i^c$  and  $R_i^l$  can be accurately expressed as

$$R_i^c = \sqrt{(x_i - X_c)^2 + (y_i - Y_c)^2 + R^2} \quad (2)$$

$$R_i^l = \sqrt{(x_i - X_l)^2 + (y_i - Y_l)^2 + R^2} \quad (3)$$

Substitute Eq. (2) and (3) into Eq. (1), and rewrite the Eq. (1) as the following matrix form

$$\mathbf{V}_{M \times 1} = \mathbf{G}_{M \times N} \cdot \mathbf{T}_{N \times 1} \quad (4)$$

Where,  $\mathbf{V}$  is the measured visibility function,  $\mathbf{T}$  is the brightness temperature image,  $\mathbf{G}$  is the imaging matrix, whose elements are

$$G(m, n) = F_{mc}(x_i, y_i) F_{ml}^*(x_i, y_i)$$

$$e^{j \frac{2\pi}{\lambda} \left[ \sqrt{(x_i - X_{ml})^2 + (y_i - Y_{ml})^2 + R^2} - \sqrt{(x_i - X_{mc})^2 + (y_i - Y_{mc})^2 + R^2} \right]} \quad (5)$$

where  $(X_{mc}, Y_{mc})$  and  $(X_{ml}, Y_{ml})$  are the coordinates of antenna pairs  $(c, l)$ , the corresponding visibility sample is  $V_m$ . For most SAIR system with fewer antennas, the dimensions of  $\mathbf{V}$  are significantly less than the ones of image  $\mathbf{T}$ . So Eq. (4) is an underdetermined equation with underdetermined  $\mathbf{G}$  matrix. Besides, the visibility function  $\mathbf{V}$  usually has some observation errors. Under this circumstance, the regularization method is one of the most effectual methods to reconstruct image  $\mathbf{T}$ . Its classic reconstruction model can be expressed as

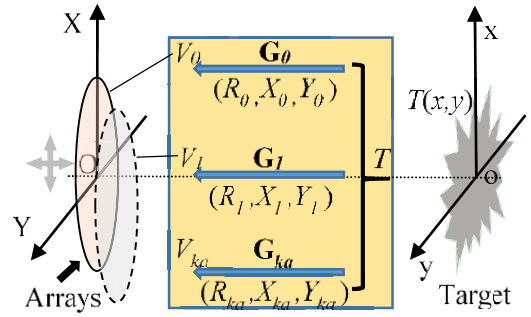


Fig. 2 Multiple imaging measurement schematic.

$$\mathbf{T}^R = \min_{\mathbf{T}} \{ \|\mathbf{GT} - \mathbf{V}\|_F^2 + \alpha P(\mathbf{T}) \} \quad (6)$$

where,  $\|\mathbf{V} - \mathbf{GT}\|_F^2$  is the fidelity term,  $P(\mathbf{T})$  is the regularization item,  $\alpha$  is the regularization parameter.

## 2.2 Super-Resolution Imaging Method

Although the MMW images can be reconstructed by the regularization method. For the most SAIR with sparse visibility functions, it will not be able to reconstruct MMW image with high accuracy. To further improve the imaging accuracy of SAIR, we propose a novel super-resolution imaging (SrI) method. In SrI method, we first utilize SAIR to detect the target at different observation locations with different distance  $R$  or array location  $(X, Y)$ . As Fig. 2 shows, the initial observation position is  $(R_0, X_0, Y_0)$ , the corresponding visibility function and imaging matrix are  $\mathbf{V}_0$  and  $\mathbf{G}_0$  respectively. Then, the antenna array will be arranged at different locations to detect the target for obtaining the visibility function  $\mathbf{V}_{ka}$ .

For a specific observation position, the imaging matrix  $\mathbf{G}_{ka}$  can be accurately expressed as

$$G_{ka}(m, n) = F_{mc}(x_i, y_i) F_{ml}^*(x_i, y_i)$$

$$e^{j \frac{2\pi}{\lambda} \left[ \frac{\sqrt{(x_i - X_{ml} - X_{ka})^2 + (y_i - Y_{ml} - Y_{ka})^2 + R_{ka}^2}}{\sqrt{(x_i - X_{mc} - X_{ka})^2 + (y_i - Y_{mc} - Y_{ka})^2 + R_{ka}^2}} \right]} \quad (7)$$

Where  $R_{ka}$  is the imaging distance,  $(X_{ka}, Y_{ka})$  is the central position of antenna array. The corresponding imaging model is

$$\mathbf{V}_{ka} = \mathbf{G}_{ka} \cdot \mathbf{T}_{ka} + \Delta \mathbf{V} \quad (8)$$

According to Eq. (6), we can easily reconstruct the image  $\mathbf{T}_{ka}$  from the above imaging model. Due to the limitation of inevitable noise  $\Delta \mathbf{V}$  and insufficient visibility  $\mathbf{V}_{ka}$ , the image  $\mathbf{T}_{ka}$  is the LR degraded image of target image  $\mathbf{T}$ . And since the different observation position, there are some small displacement and scaling between these LR images. According to these nuances, the image super-resolution fusion methods can reconstruct the target image with higher precision by interpolation and/or recombination of these LR images onto a HR image. However, many target information is lost in the process of LR image reconstruction, and the improvement is not obvious by fusing these LR images.

More importantly, since the different observation position, there are subtle differences between the measured visibility function. We can build a super-resolution imaging model with all the measured visibility functions to reconstruct the HR image directly. The corresponding super-resolution imaging model is

$$\mathbf{V}_{Srl} = \mathbf{G}_{Srl} \bullet \mathbf{T} + \Delta \mathbf{V} \quad (9)$$

Where  $\mathbf{V}_{Srl} = [\mathbf{V}_0 \dots \mathbf{V}_{ka}]'$  is the fusion visibility function,  $\mathbf{G}_{Srl} = [\mathbf{G}_0 \dots \mathbf{G}_{ka}]'$  is the fusion imaging matrix. Compared with the traditional imaging model (Eq. (4)), the dimensions of visibility function and imaging matrix are greatly improved, and the ill-conditioned problem of super-resolution imaging model is also well relieved. With more known conditions (visibility samples), the solution of Eq. (9) will be more approximate to the real MMW image  $\mathbf{T}$ .

In order to solve Eq. (9) accurately and quickly, we use the sparse optimization method to reconstruct the target image, and its reconstruction model is as follows:

$$\theta = \min_{\mathbf{T}} \{ \|\mathbf{G}_{Srl} \Psi \theta - \mathbf{V}_{Srl}\|_F^2 + \alpha \|\theta\|_{l_1} \} \quad (10)$$

Where  $\theta$  is the sparse representation of image  $\mathbf{T}$ ,  $\Psi$  is the inverse sparse transformation matrix. In this paper, we select the total-variation (TV) transform as the sparse transformation. For obtaining the optimal sparse solution  $\theta$ , the fast iterative shrinkage-thresholding algorithm (FISTA) [10] is applied to solve the optimization problem of Eq. (10). Then the final HR MMW image  $\mathbf{T}_{Srl}$  can be obtained by the following transformation.

$$\mathbf{T}_{Srl} = \Psi \theta \quad (11)$$

### 3. Simulation and Results

To evaluate the performance of SrI method, two near-field simulation experiments are made in this section. The main simulation parameters are listed in Table 1.

**Table 1** Simulation parameters of SAIR with “T” array

Parameters	Vales	Parameters	Vales
Wavelength ( $\lambda$ )	3mm	Antenna aperture ( $D_{sA}$ )	0.4m
Array size ( $M$ )	40×40	Imaging distance ( $R$ )	3–4m
Antenna spacing ( $\Delta u$ )	1 cm	Sources spacing ( $\Delta L$ )	7mm

In order to obtain a complete visibility function, the standard “T” antenna array is used in our simulation. The brightness temperature images of the target scene are shown in Figs. 3–4 (a), with their gray value as the radiation intensity of the discrete radiation sources, and the spacing ( $\Delta L$ ) between sources is set as 7mm, about one third of SAIR spatial resolution. The dimension of the target scene is 100. According to Fig. 2, we set up four observation locations, which are  $(3m, 0, 0)$ ,  $(3.3m, 0, 0.5cm)$ ,  $(3.6m, 0.5cm, 0)$  and  $(3.9m, 0.5cm, 0.5cm)$ . The corresponding visibility functions  $[\mathbf{V}_0 \mathbf{V}_1 \mathbf{V}_2 \mathbf{V}_3]$  are measured by the way of numerical simulation. The received signals of antennas are gained by integral operation of the radiation waves generated by all discrete sources, and the visibility samples are calculated by cross-correlated calculation between antennas. For comparison, the LR image  $\mathbf{T}_{Gridding}$  and  $\mathbf{T}_{TVMC}$  are first reconstructed by the Gridding method [5] and TVMC method [6] from the sparse visibility function, whose reconstructed images are shown in Figs. 3–4 (b) and (c) respectively. Then, the HR image  $\mathbf{T}_{NC}$  is reconstructed by the normalized convolution (NC) method [9] (an image fusion algorithm) from LR images  $\mathbf{T}_{TVMC}$ , and its results are shown in Figs. 3–4 (d). Finally, the HR image  $\mathbf{T}_{Srl}$  is reconstructed by the proposed SrI method from the fusion visibility function  $\mathbf{V}_{Srl}$  directly, and the results are shown in Figs. 3–4 (e).

Although the adopted  $\mathbf{G}$  matrix imaging model used in this paper has been greatly improved, some errors are still existed in the imaging model, and the sampling points of sparse visibility function are only about 16% of the pixels in target image. There are large errors in the reconstructed images  $\mathbf{T}_{Gridding}$ . As shown Figs. 3–4 (b), the noise pollution near the target and the blurred target outline can be easily observed. With the help of the total variation regularized matrix completion, the quality of image  $\mathbf{T}_{TVMC}$  is better than image  $\mathbf{T}_{Gridding}$ . As shown in Figs. 3–4 (c), its image noise is lower and the target outline is clearer. By interpolation and recombination of the image  $\mathbf{T}_{TVMC}$ , the reconstructed image  $\mathbf{T}_{NC}$  (Figs. 3–4 (d)) have higher reconstruction accuracy, since the most noise has been well removed and the target information is well restored. However, the NC method cannot effectively restore the information that has been lost in the reconstruction of LR image  $\mathbf{T}_{TVMC}$ . The clarity of image  $\mathbf{T}_{NC}$  is still poor especially for the earth scene. In SrI method, the image  $\mathbf{T}_{Srl}$  is reconstructed from the fusion visibility function  $\mathbf{V}_{Srl}$  directly and all the visi-

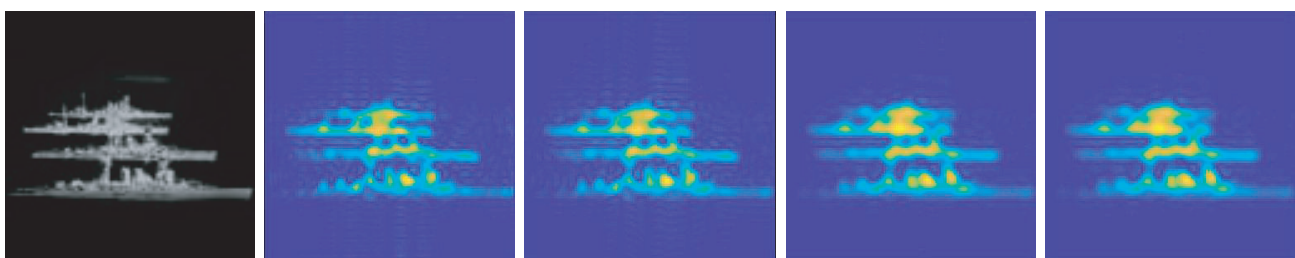


Fig.3 (a) Boats Scene.

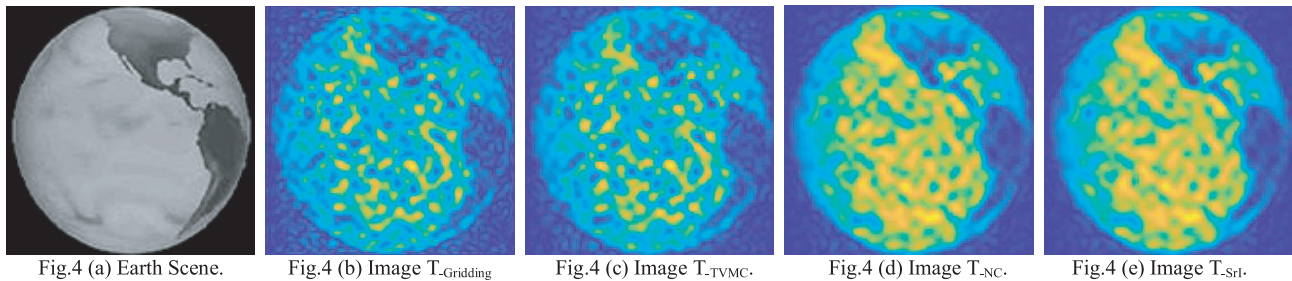
Fig.3 (b) Image  $\mathbf{T}_{Gridding}$

Fig.3 (c) Image  $\mathbf{T}_{TVMC}$ .

Fig.3 (d) Image  $\mathbf{T}_{NC}$ .

Fig.3 (e) Image  $\mathbf{T}_{Srl}$ .

**Fig. 3** The reconstructed images of Boats scene.



**Fig. 4** The reconstructed images of Earth scene.

**Table 2** Comparison of objective data between the images

Evaluation criterion	Scene	$T_{\text{-Gridding}}$	$T_{\text{-TVMC}}$	$T_{\text{-NC}}$	$T_{\text{-SrI}}$
PSNR	Boats	19.0531	19.2122	19.5939	19.6404
	Earth	13.7835	14.1511	17.6131	17.9610
SSIM	Boats	0.4529	0.4612	0.5982	0.6121
	Earth	0.2050	0.2256	0.3669	0.3837
RMSE	Boats	0.1102	0.1091	0.1031	0.0986
	Earth	0.1652	0.1563	0.1234	0.1218

bility sampling points are effectively exploited to constrain the reconstruction process, which greatly improves the accuracy of reconstructed image  $T_{\text{-SrI}}$ . In addition, the sparse reconstruction method with total variation transformation is adopted to reconstruct the image  $T_{\text{-SrI}}$  with better accuracy and clarity. As shown in Figs. 3–4(e), the image noise is well filtered out and the target information is well recovered, the clarity of image  $T_{\text{-SrI}}$  is the best.

For evaluating the accuracy of the reconstructed images, the PSNR, SSIM and RMSE are calculated as shown in Table 2. Clearly, the images of the proposed SrI method have the highest PSNR and SSIM with the lowest RMSE. This indicates that the proposed SrI method outperforms than the Gridding method, TVMC method and NC image fusion method, producing more desirable reconstruction results.

#### 4. Conclusion

To reconstruct the high-quality images from the sparse SAIR with fewer receivers, we propose a novel SrI method in this paper. By changing the observation position, more visibility sampling points can be applied to reconstruct the MMW images directly without changing the system structure of SAIR. Moreover, the super-resolution reconstruction idea is introduced in imaging inversion to restore more target information. The simulation results demonstrate that the images reconstructed by SrI method have the best accuracy and clarity. Compared with the Gridding method, TVMC method and NC fusion method, the proposed SrI method has better performance in removing image noise and extracting target information. Furthermore, because the SrI method is based on the near-field imaging model, it can also further extended in far-field imaging.

#### Acknowledgments

This work was supported by National Natural Science Foundation of China (61601237, 61671149), Natural Science Foundation of Jiangsu Province (BK20160901), Natural Science Research of Jiangsu Higher Education Institutions (16KJB420001) and NUPTSF (NY215042).

#### References

- [1] S. Demirci, H. Cetinkaya, E. Yigit, C. Ozdemir, and A. Vertiy, "A study on millimeter-wave imaging of concealed objects: Application using back-projection algorithm," *Prog Electromagn Res*, vol.128, pp.457–477, 2012.
- [2] M. Martin-Neira, D.M. LeVine, Y. Kerr, N. Skou, M. Peichl, A. Camps, I. Corbella, M. Hallikainen, J. Font, J. Wu, S. Mecklenburg, and M. Drusch, "Microwave interferometric radiometry in remote sensing: An invited historical review," *Radio Science*, vol.49, no.6, pp.415–449, June 2014.
- [3] H. Kamoda, T. Derham, T. Iwasaki, and T. Kuki, "Millimeter-wave imaging system using simultaneous frequency-encoding technique," *IEICE Trans. Electron.*, vol.E94-C, no.2, pp.206–214, Feb. 2011.
- [4] X. Zhou, H.J. Sun, J.W. He, and X. Lu, "Nufft-based iterative reconstruction algorithm for synthetic aperture imaging radiometers," *IEEE Geosci Remote S*, vol.6, no.2, pp.273–276, April 2009.
- [5] L. Feng, Q.X. Li, K. Chen, Y.F. Li, X.L. Tong, X.Q. Wang, H.L. Lu, and Y. Li, "The gridding method for image reconstruction of nonuniform aperture synthesis radiometers," *IEEE Geosci Remote S*, vol.12, no.2, pp.274–278, Feb. 2015.
- [6] Y.L. Zhang, W. Miao, Z.H. Lin, H. Gao, and S.C. Shi, "Millimeter-wave insar image reconstruction approach by total variation regularized matrix completion," *Remote Sens-Basel*, vol.10, no.7, July 2018.
- [7] J. Chen and Y. Li, "The cs-based imaging algorithm for near-field synthetic aperture imaging radiometer," *IEICE Trans. Electron.*, vol.E97-C, no.9, pp.911–914, Sept. 2014.
- [8] H.W. Lin and J. Chen, "Comparison of several hyperspectral image fusion methods for superresolution," 2018 *Ieee 3rd International Conference on Image, Vision and Computing (Icivc)*, pp.448–452, 2018.
- [9] T.Q. Pham, L.J. van Vliet, and K. Schutte, "Robust fusion of irregularly sampled data using adaptive normalized convolution," *Eurasip J Appl Sig P*, 2006.
- [10] A. Beck and M. Teboulle, "A fast iterative shrinkage-thresholding algorithm for linear inverse problems," *SIAM J Imaging Sciences*, vol.2, no.1, pp.183–202, 2009.